CrystEngComm

RSC Publishing

PAPER

Mn^{II}, Cu^{II} and Co^{II} coordination polymers showing antiferromagnetism, and the coexistence of spin frustration and long range magnetic ordering†

Cite this: *CrystEngComm*, 2013, **15**, 7756

Ya-Min Li,*[a] Chang-Yu Xiao,[a] Xu-Dong Zhang,[b] Yan-Qing Xu,[c] Hui-Jie Lun[a] and Jing-Yang Niu*[a]

Received 7th June 2013,
Accepted 31st July 2013

DOI: 10.1039/c3ce41046c

www.rsc.org/crystengcomm

Based on the ligand 1,2-H_2bdc (1,2-H_2bdc = 1,2-benzenedicarboxylic acid), three 2D coordination polymers $[Mn(1,2\text{-bdc})]_n$ (**1**), $[Cu(1,2\text{-bdc})]_n$ (**2**) and $[Co_3(OH)_2(1,2\text{-bdc})_2]_n$ (**3**), have been prepared and characterized. In comparison with the mononuclear Mn unit of compound **1**, paddle-wheel binuclear $Cu_2(CO_2)_4$ and trinuclear $Co_3(OH)$ building units are observed in **2** and **3**, respectively. Also, the bdc^{2-} ligands adopt different coordination modes in the three compounds. The resulting two frustrated lattices have been observed, such as the triangular lattice for **2** and the Kagomé lattice for **3**, and thus, both complexes **2** and **3** show spin frustrated antiferromagnetic properties. In addition, the magnetic hysteresis loops reveal the existence of the long range ordering in **2** and **3**. Comparatively, the magnetic measurements indicate that compound **1** exhibits a weak antiferromagnetic interaction, and the fit of the variable-temperature magnetic susceptibility data to the empirical equation leads to the following parameters: $J = -0.80(1)$ cm^{-1} and $g = 2.02$.

Introduction

Recently geometrically frustrated antiferromagnets have been paid considerable attention in solid state science, due to the great correlation with the ground-state behaviors such as spin liquids, spin ices and spin glasses.[1–3] Geometric spin frustration occurs only when all of the nearest neighbor interactions cannot be satisfied simultaneously,[4] which is greatly related to the structure and only observed in individual or mixed corner- and/or edge-sharing magnetic lattices such as Kagomé and triangular lattices in two-dimensional or three dimensional systems.[5,6] Investigations have been centered on the jarosite family of minerals, with the general formula $AM_3X_6(SO_4)_2$ (A = monovalent, divalent or trivalent cation, M = transition metal ion, X = OH or F), of which triangular units of $M_3(\mu_3\text{-X})$ as secondary building units construct Kagomé or triangular lattices, usually in $Fe^{II}/^{III}$, $V^{II}/^{III}$ or $Cr^{II}/^{III}$ compounds.[7] In fact, by employing carboxylic acid or *N*-heterocycle organics as the ligands, a few $M_3(\mu_3\text{-X})$ (M = Mn^{II}, Cu^{II} or Co^{II}, X = OH, O or F) spin frustration compounds have also been observed.[8] Besides these, the researches have also involved paddle wheel $M_2(CO_2)_4$ (M = Cu^{II}, Ru^{II}) dimmers positioned at the Kagomé lattice points and bridged by the ligands,[9] for example, Zaworotko and his coworkers reported the first example of a nanoscale Kagomé lattice.[9a]

Despite all of this, most magnetic materials with a spin frustration lattice do not show a phase transition to a long range ordered state, due to competing antiferromagnetic exchange interactions.[4a] In addition only several cases simultaneously containing spin frustration and long range magnetic order have been reported, which feature Kagomé-like lattices with carboxylic acid or *N*-heterocycle ligands employed.[6c,10] Among them, it has been demonstrated that the angular bifunctional carboxylate ligands such as benzene dicarboxylate or 1,2-cyclohexane-dicarboxylic acid could act as linkers to construct two-dimensional Kagomé-like lattices.[9a,10b] Inspired by the facts above, we carried out the self-assembly reactions of 1,2-H_2bdc (1,2-H_2bdc = 1,2-benzenedicarboxylic acid) and transition metal ions such as Mn^{II}, Cu^{II} or Co^{II} to obtain three 2D coordination polymers $[Mn(1,2\text{-bdc})]_n$ (**1**), $[Cu(1,2\text{-bdc})]_n$ (**2**) and $[Co_3(OH)_2(1,2\text{-bdc})_2]_n$ (**3**). Although

[a]*Henan Key Laboratory of Polyoxometalate, Institute of Molecular and Crystal Engineering, College of Chemistry and Chemical Engineering, Henan University, Kaifeng, Henan 475004, P. R. China. E-mail: liyamin@henu.edu.cn*
[b]*State Key Laboratory of Structural Chemistry, Fujian Institute of Research on the Structure of Matter, Chinese Academy of Sciences, Fuzhou, Fujian 350002, P. R. China*
[c]*School of Chemistry, Key Laboratory of Cluster Science, Ministry of Education of China, Beijing Institute of Technology, Beijing, 100081, P. R. China*

† Electronic supplementary information (ESI) available: crystallographic data (CIF), coordination modes of bdc^{2-} (Scheme S1), structural diagrams and additional graphics about physical characterizations (Fig. S1–S9), tables for the crystal data and refinement details and selected bond lengths and bond angles for the three complexes (Tables S1 and S2). These materials are available free of charge *via* the internet. CCDC reference numbers 913354–913356 for compounds **1–3** contain the supplementary crystallographic data for this paper. For ESI and crystallographic data in CIF or other electronic format see DOI: 10.1039/c3ce41046c

some compounds have been reported using 1,2-H_2bdc as the ligand,[11] here, two geometrically frustrated lattices are observed with $Cu_2(CO_2)_4$ located in the triangular lattice points of **2** and $Co_3(OH)$ in the Kagomé lattice points of **3**. As a result, both compounds **2** and **3** show the phenomena of spin frustration, as well as the existence of spin canting long range magnetic ordering. For compound **1**, the results from the magnetic measurements reveal weak antiferromagnetic interactions between the Mn(II) ions.

Results and discussion

Synthesis

In the absence of phdat (2-phenyl-4,6-diamine-triazine), an effort has been made to obtain three compounds, but it was proved invalid. Accordingly, it is inferred that phdat with two –NH_2 groups and aromatic carboxylic acid might form a buffer solution at a certain temperature and pressure and phdat played an important role in adjusting slightly the pH value.

The crystal structure of [Mn(1,2-bdc)]$_n$ (1)

The single crystal X-ray diffraction analysis revealed that complex **1** crystallized in the monoclinic space group *P*2/*c* with a 2D network built up from a mononuclear Mn unit bridged by the bdc^{2-} ligand. The Mn atoms are determined by the bond-valence calculation,[12] whose value is 2.085, suggesting that the Mn atoms are in the +2 oxidation state. The asymmetric unit of compound **1** contains a half Mn(II) ion and a half bdc^{2-} ligand. From Fig. 1a, each Mn(II) atom bears an irregular six-coordinated environment in [MnO_6], coordinated to six carboxylic oxygen atoms from five bdc^{2-} with the Mn–O distances ranging from 2.114(3) Å to 2.243(3) Å. The bdc^{2-} ligand adopts the $\eta^1{:}\eta^2{:}\eta^2{:}\eta^1{:}\mu_5$ mode to coordinate to the metal center (Scheme S1a, ESI†), which is reported for the first time. As shown in Fig. 1b, each bdc^{2-} affording two μ_2-oxygen atoms from two different carboxylic groups, links the neighboring three Mn(II) atoms, and as a result, along the *c*-axis direction, the adjacent Mn(II) atoms are linked into a one-dimensional chain structure, with an Mn···Mn separation of 3.481 Å and an Mn–O–Mn angle of approximately 104.15°.

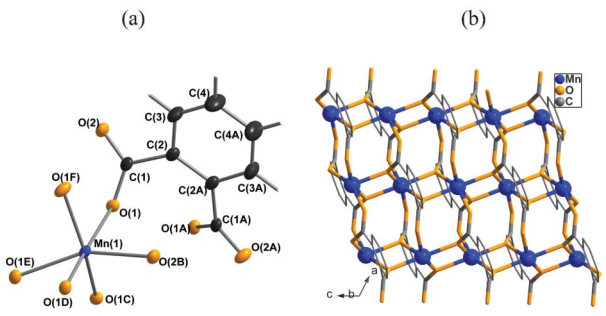

Fig. 1 (a) The coordination diagram of the metal ion with the thermal ellipsoid at the 50% probability in **1**. (b) The 2D network of **1**. Symmetry codes: A −*x*, *y*, 0.5 − *z*; B −1 + *x*, *y*, *z*; C −*x*, 1 − *y*, 1 − *z*; D −*x*, *y*, 1.5 − *z*; E *x*, 1 − *y*, 0.5 + *z*; F 1 − *x*, *y*, 1.5 − *z*.

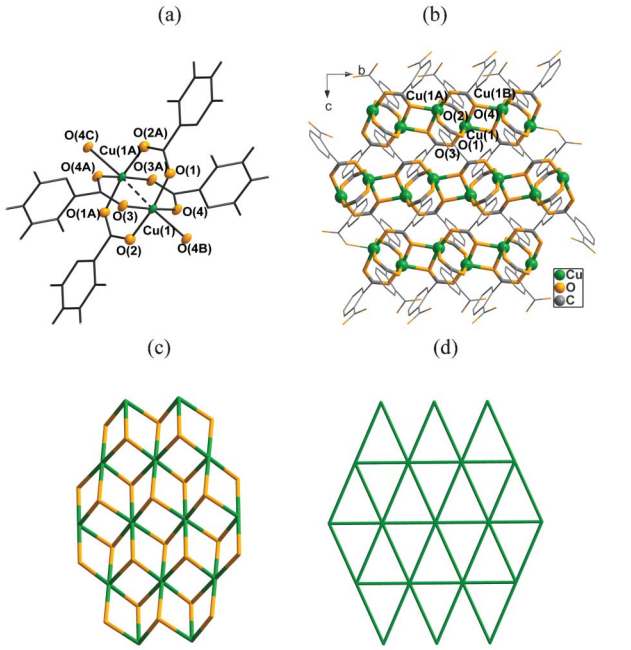

Fig. 2 (a) The binuclear unit diagram of **2** with the thermal ellipsoid at the 50% probability. (b) The 2D network of **2**. (c) A typical **Kgd** topological net with the $Cu_2(CO_2)_4$ units represented as green balls and the bdc^{2-} ligand as orange balls. (d) A geometrically frustrated triangular lattice in **2** with the $Cu_2(CO_2)_4$ units being represented as green balls. Symmetry codes: A 1 − *x*, 2 − *y*, 1 − *z*; B 1 − *x*, 3 − *y*, 1 − *z*; C *x*, −1 + *y*, *z*.

In addition, each bdc^{2-} bridges three neighboring chains into a 2D structure by two carboxylic groups. The intra-chain shortest Mn···Mn separation is 4.582 Å.

A further insight into the nature of the framework can be acquired by using topological analysis. Each Mn(II) atom coordinated to five ligands, is therefore treated as a five-connected node. The bdc^{2-} ligand behaves as a pentadentate mode to coordinate to the metal center, so that the ligand may be also considered as a five-connected node. The overall two-dimensional network is simplified as a uninodal net five-connected 2D network with the point symbol of $\{4^8.6^2\}$ (Fig. S1, ESI†).

The crystal structure of [Cu(1,2-bdc)]$_n$ (2)

Although the chemical formula of **2** is the same as that of **1**, compound **2** crystallized in the monoclinic space group *P*2(1)/*c* with the 2D network consisting of binuclear $Cu_2(CO_2)_4$ units bridged by the bdc^{2-} ligand. As shown in Fig. 2a, each asymmetric unit contains only one crystallographically independent Cu(II) ion and one bdc^{2-}. Each Cu(II) atom is coordinated to five oxygen atoms, resulting in a [CuO_5] square pyramidal configuration, of which the five oxygen atoms are from five carboxylic groups with the basal Cu–O bond lengths ranging from 1.935(3) to 2.033(3) Å, and the apical Cu–O distance of approximately 2.204(3) Å. The basal oxygen (O(1), O(2), O(3), O(4)) and Cu(1) atoms present an almost planar geometry with the mean deviation from the planarity of approximately 0.062 Å. The neighboring Cu(1) and Cu(1A) (A: 1 − *x*, 2 − *y*, 1 − *z*) atoms are bridged by four carboxylic groups,

forming a paddle-wheel shaped binuclear $Cu_2(CO_2)_4$ unit with the Cu···Cu distance of approximately 2.623 Å, which is similar to those of the reported $Cu_2(CO_2)_4$ units.[13] As shown in Fig. 2b, along the *b*-axis direction, sharing two carboxylic oxygen atoms, the neighboring binuclear $Cu_2(CO_2)_4$ units are therefore connected into a one-dimensional chain structure with a Cu(1)···Cu(1B) (B: $1-x, 3-y, 1-z$) distance of 3.26 Å (Cu–O–Cu angles of approximately 100.4°). Different from that of **1**, the bdc^{2-} ligand adopts the $\eta^1{:}\eta^1{:}\eta^1{:}\eta^2{:}\mu_5$ mode to coordinate to the metal center (Scheme S1b, ESI†). That is to say, in addition to helping the formation of the one-dimensional structure, the carboxylic groups further link the adjacent chains into a two-dimensional network.

From the view of topology, the binuclear unit $Cu_2(CO_2)_4$ is considered as a 6-connected node, and the bdc^{2-} ligand as a 3-connected node, and thus the overall structure can be described as a 2-nodal (3,6)-connected net with the point symbol of $\{4^3\}_2\{4^6.6^6.8^3\}$, which is a typical **Kgd** (Kagomé dual) topological net, known as a CdI_2 net (Fig. 2c).[14] If only considering the binuclear units $Cu_2(CO_2)_4$ as 6-connected nodes, and the bdc^{2-} ligands as linkers, the 2D framework may be described as a triangular frustrated lattice (Fig. 2d).[6]

The crystal structure of $[Co_3(OH)_2(1,2\text{-}bdc)_2]_n$ (3)

Complex **3**, crystallizing in the monoclinic space group $P2(1)/c$, exhibits a two-dimensional network, of which the trinuclear core $Co_3(OH)$ units are connected by the bdc^{2-} ligand. From Fig. 3a, the asymmetric unit of complex **3** contains two and two half crystallographically independent Co(II) ions, two hydroxyl groups and two bdc^{2-} ligands. All of the cobalt ions are assigned as divalent cations and the two μ_3-O atoms as hydroxyl oxygen atoms according to the charge balance and the BVS calculations which give values of 1.957, 2.010, 2.034, 2.025, 1.122 and 1.121 for Co(1), Co(2), Co(3), Co(4), O(9) and O(10), respectively. Co(1) is in an elongated $[CoO_6]$ octahedral configuration, coordinated to two carboxylato–O atoms from two bdc^{2-} ligands and two hydroxyl–O atoms in the equatorial direction (Co–O 2.005(3)–2.064(3) Å). It is axially coordinated to two carboxylato–O atoms from the other two bdc^{2-} ligands (Co–O 2.345(3)–2.367(3) Å). Co(2), Co(3) and Co(4) bear slightly distorted octahedral configurations, coordinated to four carboxylato–O atoms from four bdc^{2-} ligands and two hydroxyl–O atoms (Co–O 2.082(3)–2.118(3) Å). Each hydroxyl group as a μ_3 bridge links three different Co(II) atoms to the $Co_3(OH)$ core as in those of the examples $Co_3(OH)_2$(3,4-pydc)$_2(H_2O)_2$, Co_3(2,4-pydc)$_2(\mu_3\text{-}OH)_2\cdot 5H_2O$ and $[Co_3(\mu_3\text{-}OH)_2$(1,2-chdc)$_2]$.[10b,15] The $Co_3(OH)$ core can be described as a flattened tetrahedron, of which three Co^{II} atoms are located at the base with the basal edge Co···Co distances of approximately 3.114–3.533 Å, and the hydroxyl–O atom sited in the apex. As shown in Fig. 3b, by sharing six Co(II) corners, six adjacent $Co_3(OH)$ tetrahedrons (three forward and three inverted tetrahedrons) compose a hexagram, which is further connected to a beautiful 2D honeycomb layer. The bdc^{2-} ligand adopts a different $\eta^2{:}\eta^1{:}\eta^1{:}\eta^2{:}\mu_6$ mode from those of **1** and **2** to coordinate to the metal center (Scheme S1c, ESI†), and each pair of ligands decorate two sides of one hexagram, forming together a pore with an aperture approximately 2 × 3 Å, which further consolidates the overall 2D framework.

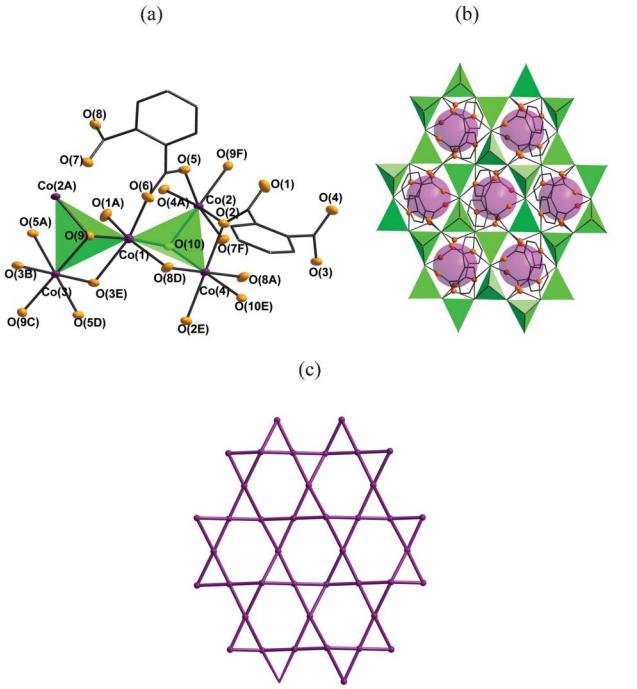

Fig. 3 (a) The metal coordination diagram with the thermal ellipsoid at the 50% probability in complex **3** (symmetry codes: A $-x, 0.5+y, 0.5-z$; B $x, 1+y, z$; C $-x, 1-y, 1-z$; D $x, 0.5-y, 0.5+z$; E $-x, -y, 1-z$; F $-x, -0.5+y, 0.5-z$). (b) A beautiful 2D honeycomb layer in **3**, the purple balls highlight the pores. (c) A geometrically frustrated Kagomé lattice in **3** with the purple balls representing Co^{II}. Green tetrahedrons representing $Co_3(OH)$ cores.

From the view of topology, if the bdc^{2-} ligand is ignored, each Co(II) can be described as a 4-connected node, and the overall 2D network may be simplified as a distorted frustrated Kagomé (**Kgm**) lattice (Fig. 3c).[5,16] However, if only considering each $Co_3(OH)$ core as a 3-connected node, the overall structure can be described as a uninodal 3-connected net with the point symbol of 6^3 (Fig. S2, ESI†), known as a **hcb** topological net.[17]

IR spectra, PXRD and thermal stability

From the IR spectra (Fig. S3, ESI†), the sharp peak at 3598 cm^{-1} of **3** should be attributed to the stretching vibration of the OH group, demonstrating the existence of the OH group in compound **3**. The antisymmetric stretching vibrations of the carboxylic groups are assigned to 1598 and 1549 cm^{-1} for **1**, 1616 and 1596 cm^{-1} for **2**, and 1625 and 1598 cm^{-1} for **3**, while the symmetric stretching vibrations at 1355 cm^{-1} for **1**, 1396 cm^{-1} for **2**, and 1390 cm^{-1} for **3**, which show the bridging modes of the carboxylic groups.[18] In order to check the phase purity of complexes **1**, **2** and **3**, powder X-ray diffraction (PXRD) patterns were recorded at room temperature (Fig. S4, ESI†). The experimental and simulated PXRD patterns agree well with each other, confirming the good phase purity. The thermogravimetric curves (Fig. S5, ESI†) show the high stability of the three compounds, which are evident from the beginning loss temperature (380 °C for **1**, 305 °C for **2**, and 370 °C for **3**).

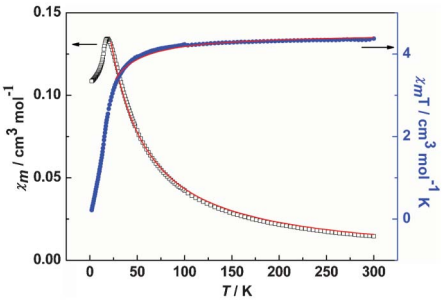

Fig. 4 The $\chi_m T$ *vs. T* and χ_m *vs. T* plots of **1** in the range of 2–300 K at 1 kOe. The solid line is the best-fit.

Magnetic properties

The $\chi_m T$ *vs. T* and χ_m *vs. T* plots of **1** in the range of 2–300 K at 1 kOe are shown in Fig. 4. The $\chi_m T$ value is 4.37 cm^3 mol^{-1} K at 300 K, which is nearly equal to the expected value of 4.38 cm^3 mol^{-1} K of one magnetically isolated spin Mn^{II} ion (S = 5/2, g = 2.0). When the temperature is lowered, the $\chi_m T$ value slightly decreases to reach the value of 3.58 cm^3 mol^{-1} K at 35 K, and then the $\chi_m T$ value rapidly decreases to 0.27 cm^3 mol^{-1} K at 2 K upon further cooling, which shows an antiferromagnetic behavior between the Mn^{II} ions. The temperature dependence of the reciprocal susceptibility (χ_m^{-1}) of **1** obeys the Curie–Weiss law in the temperature range of 300 K–25 K, giving C = 4.55 cm^3 K mol^{-1} and θ = −7.26 K, demonstrating the weak antiferromagnetic interaction. Taking into account the two-dimensional character of **1**, the plots of $\chi_m T$ *vs. T* and χ_m *vs. T* were fitted by means of the analytical expression derived by Curély for an infinite 2D square lattice composed of classical spins (S = 5/2) isotropically coupled and based on the exchange Hamiltonian $H = -\Sigma_{nn} J S_i S_j$, where S_{nn} runs over all pairs of the nearest-neighbor spins i and j (Heisenberg couplings):[18b,19]

$$\chi = [Ng^2\beta^2 S(S+1)(1+u)^2]/[3kT(1-u)^2]$$

Here, N, β, k and u represent Avogadro's number, Bohr's magneton, Boltzmann's constant, and the Langevin function:

$$u = L(JS(S+1)/kT) = \coth(JS(S+1)/kT) - kT/JS(S+1)$$

The best fitting of 20 K–300 K gave J = −0.67(1) cm^{-1}, g = 2.10 and $R = 3.1 \times 10^{-6}$ (the agreement factor defined as $R = \Sigma[(\chi_m T)_{calcd} - (\chi_m T)_{obsd}]^2/\Sigma[(\chi_m T)_{obsd}]^2$). These results indicate weak antiferromagnetic interactions between the Mn^{II} ions. Here one J value was considered. In fact, there are two sets of magnetic exchange pathways: one is a two μ_2-O bridge with Mn–O–Mn angles of 104.15°, the other consists of two *syn*, *syn*-carboxylate bridges. According to the literature,[18b,20] both exchange pathways give weak antiferromagnetic interactions, suggesting that the one average J value adopted is similar and relatively reasonable. Additionally, the curve of magnetization *vs.* the applied field at 2 K is shown in Fig. S6, ESI.† The magnetization is only 0.83 Nβ at 3.5 T, which is far below the saturation value of 5 Nβ which is expectedfor one Mn^{II} ion (S = 5/2, g = 2).

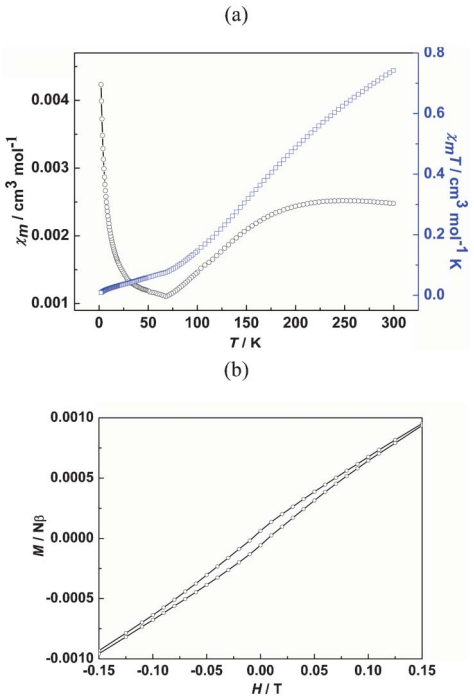

Fig. 5 (a) The $\chi_m T$ *vs. T* and χ_m *vs. T* plots of **2** in the range of 2–300 K at 1 kOe. (b) The magnetic hysteresis loop of **2**.

For **2**, upon 1 kOe, the plots of $\chi_m T$ *vs. T* and χ_m *vs. T* are shown in Fig. 5a (from 300 K to 2 K). At 300 K, the $\chi_m T$ value (0.74 cm^3 mol^{-1} K) of each Cu_2 unit is close to that expected for two magnetically isolated Cu^{II} S = 1/2 spin carriers (0.75 cm^3 mol^{-1} K). Upon cooling, the $\chi_m T$ value of 0.076 cm^3 mol^{-1} K at 69 K is obtained, and this gradually approaches 0.009 cm^3 mol^{-1} K at 2 K, which is indicative of an antiferromagnetic interaction. The χ_m value shows a maximum below 300 K and a minimum at around 69 K, followed an upturn at a lower temperature, also suggesting that antiferromagnetic coupling predominates in **2** as well as the existence of the ferromagnetic state or uncompensated paramagnetic moments below 69 K, which can be understood in terms of the magnetic interactions governed by intra- and interdimer coupling.[9a,b] It is further demonstrated about the ferromagnetic state that a hysteresis loop is observed (Fig. 5b), which is consistent to the upturn in the susceptibility at temperatures below 69 K. The magnetic behaviors are very similar to those of the reported Kagomé lattice $[(Cu_2(py)_2(bdc)_2)_3]_n$,[9a,b] which are ascribed to the spin frustrated antiferromagnetic state, which is consistent with the geometrically frustrated triangular lattice. It is inferred that the weak ferromagnetic state originates from spin canting which results from the disruption of perfect antiferromagnetic ordering by introducing spin frustration to the triangular lattice. The magnetization is 0.018 Nβ at 5 T, which is far smaller than that of the expected saturation value of 2 Nβ for two isolated Cu^{II} ions (S = 1/2, g = 2) (Fig. S7, ESI†).

For **3**, the temperature-dependent magnetic susceptibilities were measured at different external fields (Fig. 6a). At 300 K, the $\chi_m T$ value is 8.01 cm^3 mol^{-1} K, which is significantly higher than the expected value of 5.63 cm^3 mol^{-1} K of three

magnetically isolated spin Co^{II} ions with $S = 3/2$, indicating a large orbital contribution arising from the high-spin octahedral Co^{II} centers. At a 1 kOe field, on lowering the temperature, $\chi_m T$ undergoes a gradual decrease to 2.02 cm^3 mol^{-1} K (10 K), where a sharp minimum is observed. With further cooling, $\chi_m T$ increases rapidly to reach a maximum value of 8.85 cm^3 mol^{-1} K at about 7 K and then drops abruptly again. The decrease is due to the spin–orbit coupling of Co^{II} or antiferromagnetic coupling, while the increase indicates a long-range ferromagnet ordering, which may be caused by the spin canting. However, upon increasing the external magnetic fields, the maximum of $\chi_m T$ becomes broader and lower and disappears finally (at 10 kOe). The temperature dependence of the reciprocal susceptibility (χ_m^{-1}) above 50 K obeys the Curie–Weiss law with $C = 10$ cm^3 mol^{-1} K, and $\theta = -70.9$ K, indicating dominant antiferromagnetic interactions (Fig. S8, ESI†). The above magnetic behaviors are similar to those of the Kagomé-like lattice $[Co_3(\mu_3\text{-}OH)_2(1,2\text{-}chdc)_2]$,[10b] showing a spin frustration in **3**, of which the degree can be quantified by $f = |\theta/T_N| = 7.1$ ($T_N = 10$ K defined by the maximum of $d(\chi_m T)/dT$, Fig. S9, ESI†), indicating the presence of moderate spin frustration in **3**,[5,6] which is consistent to the frustrated Kagomé lattice.

To fully characterize the long-range ferromagnetic ordering resulting from spin canting, field-cooled magnetizations (FCM) and zero-field-cooled magnetizations (ZFCM) were measured at 100 Oe, 50 Oe and 10 Oe (Fig. 6b). It is observed that the divergence occurs below 11 K for the ZFCM and FCM curves upon different fields, indicating the existence of remnant magnetization, which is also further confirmed by a characteristic hysteresis loop at 2.0 K. From Fig. 6c, a remnant magnetization (M_r) of 0.12 Nβ and a coercive field (H_c) of 2700 Oe are observed, demonstrating the existence of the ferromagnetic state. The magnetization at 2 K gradually increases to 2.4 Nβ at 8 T, but is far from the saturation value ($M_s = 6.5$ Nβ) for three octahedral Co^{II} ions with $S_{eff} = 1/2$ and $g = 4.33$,[21] which is consistent with the observed spin canting behavior. The canting angle is related to M_r and M_s through $\sin(\alpha) = M_r/M_s$ and is estimated to be 1.03°.[22]

The temperature dependence of the ac susceptibility measured in a field of 3 Oe also shows the same feature (Fig. 6d). The maximum of χ' observed at $T_N = 10$ K, is in agreement with the above results, and confirms the occurrence of a phase transition. The absence of an out-of-phase signal (χ'') at this temperature may be ascribed to the small magnetic moment from canting (small canting angle),[23] so that the loss of energy related to the out-of-phase signal (χ'') is negligible. The same ac susceptibility behavior has also been observed for other 2D or 3D Co^{II} complexes.[24] No frequency dependence of these transitions is observed, which precludes the possibility of a spin-glass.

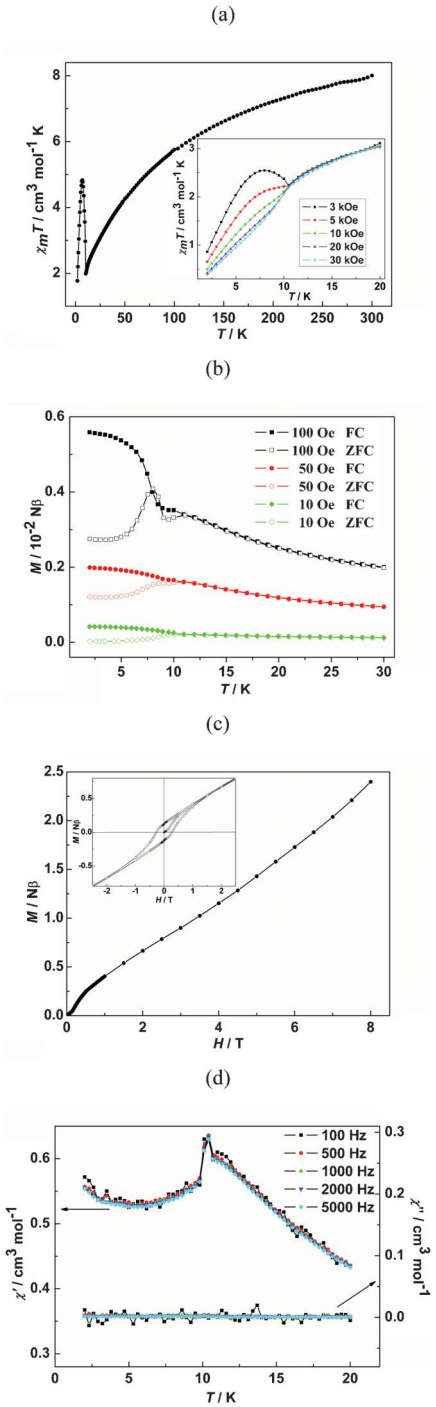

Fig. 6 (a) The $\chi_m T$ *vs.* T plot of **3** in the range of 2–300 K at 1 kOe; inset: the $\chi_m T$ *vs.* T plots at different external fields. (b) The FCM and ZFCM curves at 10 Oe, 50 Oe and 100 Oe for **3**. (c) The magnetic hysteresis loop of **3**; inset: the field-dependent magnetization of **3** at 2 K. (d) Plots of the temperature dependence of the ac susceptibility χ' and χ'' obtained at 3 Oe field for **3**.

Experimental section

Materials and physical measurements

All materials were commercially available and used as received. Infrared spectra were recorded on a Nicolet magna 750 FT-IR spectrophotometer using KBr pellets in the range of 400–4000 cm^{-1}. Elemental analyses were performed *via* Vario EL III Etro Elemental Analyzer. Thermogravimetric analyses (TGA) were performed under atmosphere with a heating rate of 10 °C min^{-1} using TGA/SDTA851e. Powder X-ray diffraction (PXRD) patterns were recorded on a Philips X'PertPro

instrument with Cu Kα radiation (λ = 1.54056 Å) in the range 2θ = 5–40° at room temperature. Magnetic measurements were carried out on a Quantum Design MPMS-XL SQUID magnetometer, and diamagnetic corrections were estimated from Pascal's constants.

The synthesis of complex [Mn(1,2-bdc)]$_n$

A mixture of $MnCl_2{\cdot}4H_2O$ (0.396 g, 2 mmol), 1,2-H_2bdc (0.166 g, 1 mmol), phdat (0.150 g, 0.8 mmol) and H_2O (10 mL) was placed in a Teflon-lined stainless steel vessel, heated to 150 °C for 3 days, then cooled to room temperature. Pink strip crystals of **1** were obtained and washed with H_2O (yield: 0.165 g, 75.3% based on 1,2-H_2bdc). Elemental analysis (%): calcd for C 43.86, H 1.84. Found C 43.61, H 1.79. IR (KBr, cm^{-1}): 3428 m, 1598 w, 1549 s, 1483 w, 1425 m, 1355 m, 1259 w, 1139 m, 1085 w, 954 w, 857 m, 826 w, 807 m, 733 s, 695 s.

The synthesis of complex [Cu(1,2-bdc)]$_n$

After the replacement of the $MnCl_2{\cdot}4H_2O$ in **1** by $Cu(NO_3)_2{\cdot}3H_2O$ (0.483 g, 2 mmol), and a temperature change to 120 °C, green strip crystals of **2** were obtained (yield: 0.085 g, 37.3% based on 1,2-H_2bdc). Elemental analysis (%): calcd for C 42.21, H 1.77. Found C 42.35, H 1.66. IR (KBr, cm^{-1}): 3430 m, 1616 s, 1596 s, 1526 m, 1497 w, 1451 m, 1418 w, 1396 s, 1149 m, 1091 w, 868 w, 839 w, 766 s, 711 s, 662 m.

The synthesis of complex [$Co_3(OH)_2$(1,2-bdc)$_2$]$_n$

The procedure is similar to that of **1**, except that $MnCl_2{\cdot}4H_2O$ was replaced by $CoCl_2{\cdot}6H_2O$ (0.476 g, 2 mmol), and the mixture was kept at 180 °C for 3 days. Purple strip crystals of **3** were obtained (yield: 0.114 g, 42.3% based on 1,2-H_2bdc). Elemental analysis (%): calcd for C 35.65, H 1.87. Found C 35.75, H 1.74. IR (KBr, cm^{-1}): 3598 m, 3421 m, 1625 s, 1598 s, 1501 w, 1426 w, 1390 s, 1162 w, 1097 w, 807 m, 767 w, 743 m, 695 m.

Crystallographic data collection and refinement

X-ray single crystal data were collected at 296(2) K on a Bruker Apex-II CCD areadetector diffractometer with Mo Kα radiation (λ = 0.71073 Å). Data reductions and absorption corrections were made with empirical methods. These structures were solved by direct methods using SHELXS-97[25] and refined by full matrix least-squares methods using SHELXL-97.[26] Anisotropic displacement parameters were refined for all non-hydrogen atoms. All hydrogen atoms bonded to C atoms were added in the riding model while the hydrogen atoms of the hydroxyl groups in **3** were located from the difference Fourier maps. The crystal data and refinement details for the three complexes are listed in Table S1, ESI.† The selected bond lengths and angles of compounds **1–3** are listed in Table S2, ESI.†

Conclusions

In conclusion, three different 2D frameworks [Mn(1,2-bdc)]$_n$ (**1**), [Cu(1,2-bdc)]$_n$ (**2**) and [$Co_3(OH)_2$(1,2-bdc)$_2$]$_n$ (**3**) with 1,2-H_2bdc have been achieved, which consist of mononuclear Mn, binuclear $Cu_2(CO_2)_4$ and trinuclear $Co_3(OH)$ units, respectively, and exhibit different topologies such as the geometrically frustrated triangular lattice in **2** and the Kagomé lattice in **3**. Accordingly, different magnetic behaviors have been observed in the three compounds. Compounds **2** and **3** show the coexistence of geometric spin frustration and spin canting long range magnetic ordering. In comparison, a weak antiferromagnetic interaction has been observed in compound **1**.

Acknowledgements

This research is supported by the National Science Foundation of China (21271025), the National Science Foundation of the Education Department of Henan Province (2011A150004, 12B150004), the Department of Science and Technology of Henan Province (122102210174), and the State Key Laboratory of Structural Chemistry (20110008).

Notes and references

1 (*a*) L. Balents, *Nature*, 2010, **464**, 199; (*b*) Y. Okamoto, M. Nohara, H. Aruga-Katori and H. Takagi, *Phys. Rev. Lett.*, 2007, **99**, 137207; (*c*) S. Yamashita, Y. Nakazawa, M. Oguni, Y. Oshima, H. Nojiri, Y. Shimizu, K. Miyagawa and K. Kanoda, *Nat. Phys.*, 2008, **4**, 459.

2 (*a*) S. T. Bramwell and M. J. P. Gingras, *Science*, 2001, **294**, 1495; (*b*) R. F. Wang, C. Nisoli, R. S. Freitas, J. Li, W. McConville, B. J. Cooley, M. S. Lund, N. Samarth, C. Leighton, V. H. Crespi and P. Schiffer, *Nature*, 2006, **439**, 303.

3 J. A. Mydosh, *Spin Glasses: An Experimental Introduction*, Taylor & Francis, London, 1993.

4 (*a*) J. E. Greedan, *J. Mater. Chem.*, 2001, **11**, 37; (*b*) M. P. Shores, B. M. Bartlett and D. G. Nocera, *J. Am. Chem. Soc.*, 2005, **127**, 17986.

5 (*a*) E. A. Nytko, J. S. Helton, P. Müller and D. G. Nocera, *J. Am. Chem. Soc.*, 2008, **130**, 2922; (*b*) M. U. Anwar, L. K. Thompson and L. N. Dawe, *Dalton Trans.*, 2011, **40**, 1437; (*c*) S. K. Pati and C. N. R. Rao, *Chem. Commun.*, 2008, 4683; (*d*) H. Yoshida, Y. Michiue, E. Takayama-Muromachi and M. Isobe, *J. Mater. Chem.*, 2012, **22**, 18793.

6 (*a*) M.-H. Whangbo, D. Dai, K.-S. Lee and R. K. Kremer, *Chem. Mater.*, 2006, **18**, 1268; (*b*) J. N. Behera, G. Paul, A. Choudhury and C. N. R. Rao, *Chem. Commun.*, 2004, 456; (*c*) P. Mahata, D. Sen and S. Natarajan, *Chem. Commun.*, 2008, 1278.

7 (*a*) B. M. Bartlett and D. G. Nocera, *J. Am. Chem. Soc.*, 2005, **127**, 8985; (*b*) D. G. Nocera, B. M. Bartlett, D. Grohol, D. Papoutsakis and M. P. Shores, *Chem.–Eur. J.*, 2004, **10**, 3850; (*c*) J. Frunzke, T. Hansen, A. Harrison, J. S. Lord, G. S. Oakley, D. Visser and A. S. Wills, *J. Mater. Chem.*, 2001, **11**, 179; (*d*) D. Grohol, K. Matan, J.-H. Cho, S.-H. Lee, J. W. Lynn, D. G. Nocera and Y. S. Lee, *Nat. Mater.*, 2005, **4**, 323; (*e*) G. Paul, A. Choudhury and C. N. R. Rao, *Chem. Commun.*, 2002, 1904; (*f*) C. N. R. Rao, E. V. Sampathkumaran, R. Nagarajan, G. Paul, J. N. Behera and A. Choudhury, *Chem. Mater.*, 2004, **16**, 1441.

8 (*a*) E.-Q. Gao, N. Liu, A.-L. Cheng and S. Gao, *Chem. Commun.*, 2007, 2470; (*b*) J. Tao, Y.-Z. Zhang, Y.-L. Bai and O. Sato, *Inorg. Chem.*, 2006, **45**, 4877; (*c*) S. Ferrer, F. Lloret,

I. Bertomeu, G. Alzuet, J. Borrás, S. García-Granda, M. Liu-González and J. G. Haasnoot, *Inorg. Chem.*, 2002, **41**, 5821.
9 (*a*) B. Moulton, J.-J. Lu, R. Hajndl, S. Hariharan and M. J. Zaworotko, *Angew. Chem., Int. Ed.*, 2002, **41**, 2821; (*b*) H. Srikanth, R. Hajndl, B. Moulton and M. J. Zaworotko, *J. Appl. Phys.*, 2003, **93**, 7089; (*c*) J. J. Perry, G. J. McManus and M. J. Zaworotko, *Chem. Commun.*, 2004, 2534; (*d*) J. L. Atwood, *Nat. Mater.*, 2002, **1**, 91; (*e*) S. Furukawa, M. Ohba and S. Kitagawa, *Chem. Commun.*, 2005, 865; (*f*) B. Liu, Y.-Z. Li and L.-M. Zheng, *Inorg. Chem.*, 2005, **44**, 6921.
10 (*a*) X.-Y. Wang, L. Wang, Z.-M. Wang and S. Gao, *J. Am. Chem. Soc.*, 2006, **128**, 674; (*b*) Y.-Z. Zheng, M.-L. Tong, W.-X. Zhang and X.-M. Chen, *Chem. Commun.*, 2006, 165; (*c*) E.-C. Yang, Z.-Y. Liu, Y.-L. Li, J.-Y. Wang and X.-J. Zhao, *Dalton Trans.*, 2011, **40**, 8513; (*d*) E.-C. Yang, Z.-Y. Liu, X.-Y. Wu, H. Chang, E.-C. Wang and X.-J. Zhao, *Dalton Trans.*, 2011, **40**, 10082.
11 (*a*) Y.-C. Ou, W.-T. Liu, J.-Y. Li, G.-G. Zhang, J. Wang and M.-L. Tong, *Chem. Commun.*, 2011, **47**, 9384; (*b*) S.-Y. Yang, L.-S. Long, R.-B. Huang, L.-S. Zheng and S. W. Ng, *Acta Crystallogr., Sect. C: Cryst. Struct. Commun.*, 2003, **59**, m456; (*c*) E. K. Brechin, A. Graham, A. Parkin, S. Parsons, A. M. Seddon and R. E. P. Winpenny, *J. Chem. Soc., Dalton Trans.*, 2000, 3242; (*d*) C. Y. Wang, Z. M. Wilseck, R. M. Supkowski and R. L. LaDuca, *CrystEngComm*, 2011, **13**, 1391; (*e*) Q. Yang, X.-F. Zhang, J.-P. Zhao, B.-W. Hu and X.-H. Bu, *Cryst. Growth Des.*, 2011, **11**, 2839; (*f*) J.-W. Cheng, S.-T. Zheng and G.-Y. Yang, *Inorg. Chem.*, 2007, **46**, 10261–10267; (*g*) P.-C. Cheng, P.-T. Kuo, Y.-H. Liao, M.-Y. Xie, W. Hsu and J.-D. Chen, *Cryst. Growth Des.*, 2013, **13**, 623–632.
12 I. D. Brown and D. Altermatt, *Acta Crystallogr., Sect. B: Struct. Sci.*, 1985, **41**, 244.
13 (*a*) S. Takamizawa, E. Nakata, T. Akatsuka, R. Miyake, Y. Kakizaki, H. Takeuchi, G. Maruta and S. Takeda, *J. Am. Chem. Soc.*, 2010, **132**, 3783; (*b*) S. A. Bourne, J.-J. Lu, A. Mondal, B. Moulton and M. J. Zaworotko, *Angew. Chem., Int. Ed.*, 2001, **40**, 2111; (*c*) S. S.-Y. Chui, S. M.-F. Lo, J. P. H. Charmant, A. G. Orpen and I. D. Williams, *Science*, 1999, **283**, 1148; (*d*) D. Maspoch, D. Ruiz-Molina and J. Veciana, *J. Mater. Chem.*, 2004, **14**, 2713.
14 (*a*) S.-R. Zheng, Q.-Y. Yang, Y.-R. Liu, J.-Y. Zhang, Y.-X. Tong, C.-Y. Zhao and C.-Y. Su, *Chem. Commun.*, 2008, 356; (*b*) N. Wang, J.-G. Ma, W. Shi and P. Cheng, *CrystEngComm*, 2012, **14**, 5198; (*c*) M.-Y. Zhang, W.-J. Shan and Z.-B. Han, *CrystEngComm*, 2012, **14**, 1568; (*d*) E. Y. Choi, P. M. Barron, R. W. Novotney, C.-H. Hu, Y. U. Kwon and W. Y. Choe, *CrystEngComm*, 2008, **10**, 824.
15 (*a*) M.-L. Tong, S. Kitagawa, H.-C. Chang and M. Ohba, *Chem. Commun.*, 2004, 418; (*b*) Z.-G. Li, G.-H. Wang, H.-Q. Jia, N.-H. Hu and J.-W. Xu, *CrystEngComm*, 2008, **10**, 173.
16 X. Feng, J. Wang, B. Liu, L. Wang, J. Zhao and S. Ng, *Cryst. Growth Des.*, 2012, **12**, 927.
17 (*a*) J. Jin, S.-Y. Niu, Q. Han and Y.-X. Chi, *New J. Chem.*, 2010, **34**, 1176; (*b*) M. Ahmad, R. Das, P. Lama, P. Poddar and P. K. Bharadwaj, *Cryst. Growth Des.*, 2012, **12**, 4624; (*c*) S.-S. Chen, Y. Zhao, J. Fan, T. Okamura, Z.-S. Bai, Z.-H. Chen and W.-Y. Sun, *CrystEngComm*, 2012, **14**, 3564; (*d*) Y. Gong, J.-H. Li, T. Wu, J.-B. Qin, R. Cao and J. Li, *CrystEngComm*, 2012, **14**, 663; (*e*) J.-J. Jang, L. Li, T. Yang, D.-B. Kuang, W. Wang and C.-Y. Su, *Chem. Commun.*, 2009, 2387.
18 (*a*) X.-J. Li, X.-Y. Wang, S. Gao and R. Cao, *Inorg. Chem.*, 2006, **45**, 1508; (*b*) T. K. Maji, S. Sain, G. Mostafa, T.-H. Lu, J. Ribas, M. Monfort and N. R. Chaudhuri, *Inorg. Chem.*, 2003, **42**, 709; (*c*) X.-Y. Yi, H.-C. Fang, Z.-G. Gu, Z.-Y. Zhou, Y.-P. Cai, J. Tian and P. K. Thallapally, *Cryst. Growth Des.*, 2011, **11**, 2824.
19 (*a*) J. Curély, *Phys. B*, 1998, **245**, 263; (*b*) J. Curély, *Phys. B*, 1998, **254**, 277; (*c*) J. Curély and J. Rouch, *Phys. B*, 1998, **254**, 298; (*d*) Z. Chen, D.-L. Gao, C.-H. Diao, Y. Liu, J. Ren, J. Chen, B. Zhao, W. Shi and P. Cheng, *Cryst. Growth Des.*, 2012, **12**, 1201.
20 C. Desroches, G. Pilet, S. A. Borshch, S. Parola and D. Luneau, *Inorg. Chem.*, 2005, **44**, 9112.
21 (*a*) P. Yin, S. Gao, L.-M. Zheng, Z. Wang and X.-Q. Xin, *Chem. Commun.*, 2003, 1076; (*b*) H.-P. Jia, W. Li, Z.-F. Ju and J. Zhang, *Chem. Commun.*, 2008, 371.
22 (*a*) O. Kahn, *Molecular Magnetism*, VCH, New York, 1993; (*b*) R. L. Carlin, *Magnetochemistry*, Springer-Verlag, Berlin, Germany, 1986; (*c*) J. Boonmak, M. Nakano, N. Chaichit, C. Pakawatchai and S. Youngme, *Inorg. Chem.*, 2011, **50**, 7324.
23 (*a*) J. W. Yoon, S. H. Jhung, Y. K. Hwang, S. M. Humphrey, P. T. Wood and J.-S. Chang, *Adv. Mater.*, 2007, **19**, 1830; (*b*) B.-L. Chen, S.-Q. Ma, F. Zapata, F. R. Fronczek, E. B. Lobkovsky and H.-C. Zhou, *Inorg. Chem.*, 2007, **46**, 1233.
24 (*a*) Y.-Q. Tian, C.-X. Cai, X.-M. Ren, C.-Y. Duan, Y. Xu, S. Gao and X.-Z. You, *Chem.–Eur. J.*, 2003, **9**, 5673; (*b*) J.-R. Li, Q. Yu, Y. Tao, X.-H. Bu, J. Ribas and S. R. Batten, *Chem. Commun.*, 2007, 2290.
25 G. M. Seldrick, *SHELXS-97, Program for X-ray Crystal Structure Solution*, University of Göttingen, Göttingen, Germany, 1997.
26 G. M. Sheldrick, *SHELXL-97, Program for X-ray Crystal Structure Refinement*, University of Göttingen, Göttingen, Germany, 1997.

